Interface microstructure engineering by high power impulse magnetron sputtering for the enhancement of adhesion

A. P. Ehiasarian[a)]
Materials and Engineering Research Institute, Sheffield Hallam University, Howard Street, Sheffield S1 1WB, United Kingdom

J. G. Wen and I. Petrov
Frederick Seitz Materials Research Laboratory, University of Illinois, Urbana, Illinois 61801 and Materials Science Department, University of Illinois, Urbana, Illinois 61801

(Received 29 November 2006; accepted 4 January 2007; published online 2 March 2007)

An excellent adhesion of hard coatings to steel substrates is paramount in practically all application areas. Conventional methods utilize Ar glow etching or cathodic arc discharge pretreatments that have the disadvantage of producing weak interfaces or adding droplets, respectively. One tool for interface engineering is high power impulse magnetron sputtering (HIPIMS). HIPIMS is based on conventional sputtering with extremely high peak power densities reaching 3 kW cm^{-2} at current densities of >2 A cm^{-2}. HIPIMS of Cr and Nb was used to prepare interfaces on 304 stainless steel and M2 high speed steel (HSS). During the pretreatment, the substrates were biased to $U_{bias}=-600$ V and $U_{bias}=-1000$ V in the environment of a HIPIMS of Cr and Nb plasma. The bombarding flux density reached peak values of 300 mA cm^{-2} and consisted of highly ionized metal plasma containing a high proportion of Cr^{1+} and Nb^{1+}. Pretreatments were also carried out with Ar glow discharge and filtered cathodic arc as comparison. The adhesion was evaluated for coatings consisting of a 0.3 μm thick CrN base layer and a 4 μm thick nanolayer stack of CrN/NbN with a period of 3.4 nm, hardness of $HK_{0.025}=3100$, and residual stress of −1.8 GPa. For HIPIMS of Cr pretreatment, the adhesion values on M2 HSS reached scratch test critical load values of $L_C=70$ N, thus comparing well to $L_C=51$ N for interfaces pretreated by arc discharge plasmas and to $L_C=25$ N for Ar etching. Cross sectional transmission electron microscopy studies revealed a clean interface and large areas of epitaxial growth in the case of HIPIMS pretreatment. The HIPIMS pretreatment promoted strong registry between the orientation of the coating and polycrystalline substrate grains due to the incorporation of metal ions and the preservation of crystallinity of the substrate. Evidence and conditions for the formation of cube-on-cube epitaxy and axiotaxy on steel and γ-TiAl substrates are presented. © *2007 American Institute of Physics*.
[DOI: 10.1063/1.2697052]

INTRODUCTION

The adhesion of coatings to the substrates is a key factor determining their performance in a specific application and successful implementation in industrial production. The adhesion on substrates such as low- and high-carbon steels, metallic alloys, and carbides is influenced by a number of factors. One of the most important is surface contamination in the form of surface oxides and organic substances from the environment which may prevent direct contact and bonding between the film and the substrate. Films growing on top of contaminated areas have poor adhesion as the bonding to the substrates relies predominantly on the weak van der Waals forces. Furthermore, islands of contamination cause shadowing, formation of large-scale growth defects, and associated film porosity. When contaminants are removed, the crystalline substrate provides a defined chemistry that allows metallic, ionic, and covalent bonds to be established directly with the growing film.

The adhesion strength of the interface can be further improved by incorporation of metal into the substrate. It has been shown[1,2] that even 5–15 nm thick metal implanted zones can improve the adhesion of nitride films on steel and WC substrates by providing a gradient change in stress.

In order to remove contaminants, physical vapor deposition (PVD) processes typically incorporate a pretreatment step prior to coating deposition. Traditionally, the pretreatment is performed in Ar glow discharge plasmas whereby contamination is sputtered away by bombardment of gas ions which are accelerated to several hundred eV by a high bias voltage on the substrates. The plasma density n_{pl} generated is of the order of 10^8 cm^{-3} and the ion flux to the substrates j_S is in the range <0.1 mA cm^{-2}. The method can be implemented easily in industrial processes as Ar is often one of the process gases already installed. However, one disadvantage is that carbon-based contaminants have a low yield of physical sputtering in Ar. Chemical sputtering with oxygen is far superior since carbon is released into the chamber as volatile CO and CO_2. The physical sputtering yield of carbon is typically an order of magnitude lower than that of metals, and therefore surface roughening may develop as contaminated regions are sputtered slower and thus remain higher than initially clean regions. Another disadvantage is the incorpo-

[a)]Electronic mail: a.ehiasarian@shu.ac.uk

ration of the gas ions into the substrate. As Ar is inert it occupies interstitial sites whose presence induces increased strains in the substrate lattice. The high strain embrittles the substrate material by bringing it closer to its yield stress. Furthermore, when heated during pretreatment or under exploitation, Ar diffuses and agglomerates into bubbles, which introduce porosity and weakening of the interface.

In order to create sufficient Ar bombardment flux, the plasma density during Ar pretreatment is often enhanced by working at high gas pressures of the order of 10^{-2} mbar and/or by utilizing a radio frequency (rf) or midfrequency (MF) bipolar pulsing discharge. The plasma density n_{pl} achieved with rf and bipolar pulsing is of the order of 10^9 cm^{-3}, and the ion flux to the substrates j_S is in the range of 0.1–1 mA cm^{-2}. The higher flux allows faster and more efficient cleaning of the substrate and avoids oxide formation. A disadvantage in the use of rf discharge systems is that their operation depends strongly on the load of the system. This complicates process control and may result in reproducibility issues.

Superior adhesion can be obtained when etching in cathodic arc (CA) discharge environment.[2,3,15] Cathodic vacuum arc discharges are characterized with high plasma densities at the substrate of $n_{pl}=10^{10}$ cm^{-3} and j_S is in the range of 1–10 mA cm^{-2}. CAs produce a highly ionized metal flux (up to 100% when combined with a filter) and may be operated without intentionally introduced process gas. It has been shown that interfaces prepared with arc etching have a high density and contain a 3–15 nm thick implantation zone in the substrate surface for substrate bias $U_{bias} \leqslant 1.2$ kV. Such interfaces have been shown to promote localized epitaxial growth of the coating over individual grains of polycrystalline steel and WC substrates.[4] The disadvantage of unfiltered cathodic vacuum arc discharges is the production of liquid metal droplets with sizes of 100–1000 nm at the cathode. When embedded in the growing films, these macroparticles shadow the deposition flux, thus creating porosity and nucleating a larger scale growth defect as the coating thickness increases.[5]

High power impulse magnetron sputtering[6] (HIPIMS) has been shown to produce high ion fluxes with a high metal content similar to an arc discharge. HIPIMS is an impulse (short pulse) sputtering method where the peak power on the target reaches 3 kW cm^{-2} at a target current density of 2 A cm^{-2}. During the peak of the pulse $j_S=50-500$ mA cm^{-2} and $n_{pl}=10^{13}$ cm^{-3}. Fluxes generated by HIPIMS comprise high fractions of metal ions[7] with gas ion to metal ion ratios of 1:1.[8] Because it is a sputtering method, HIPIMS has the advantage that it does not produce droplets. It has been shown that single layer CrN films pretreated by HIPIMS have an excellent adhesion and superior performance in mechanical testing.[9,10] Nanoscale multilayer CrN/NbN films have also been deposited on industrial scale machines with improved adhesion and corrosion protection properties following HIPIMS pretreatment.[11]

HIPIMS has been shown to provide a powerful tool for substrate etching[9,12] and interface engineering. However, atomic level insight on the interfacial structure and chemistry produced by this method is still missing. The current paper presents results from high-resolution transmission electron microscope (TEM) analysis of the microstructure of interfaces prepared by HIPIMS and the subsequent growth of the film, which are compared with interfaces prepared by filtered cathodic vacuum arc. A CrN/NbN nanoscale multilayer coating is utilized as a model system. The adhesion of HIPIMS pretreated coatings is compared with that of Ar glow and cathodic arc pretreated benchmark coatings. We show that the crystallinity of the substrate grains is preserved during cleaning. The substrate surface is highly reactive and allows nucleation to proceed uniformly and in an oriented fashion over large areas where the bonding chemistry between coating and substrate is not disturbed by contamination. A high degree of local epitaxial growth is achieved using the HIPIMS technique for pretreatment and deposition that is comparable in nature to the interfaces obtained by CAs, but without the droplet problem encountered in an unfiltered arc and the limited productivity and upscalability of a filtered arc.

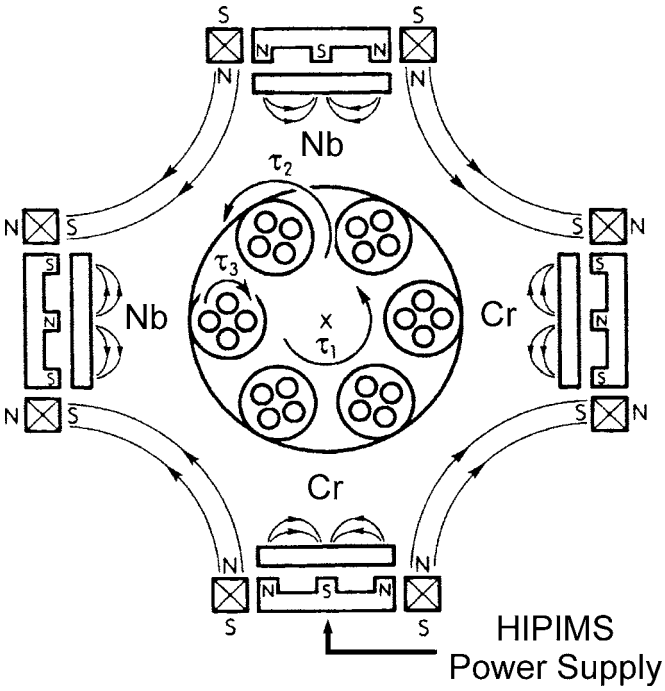

FIG. 1. Cross sectional schematic of the Hauzer HTC 1000/4 ABS coating deposition unit.

EXPERIMENTAL DETAILS

Pretreatment by high power impulse magnetron sputtering (HIPIMS)

The experiments with HIPIMS pretreatment were carried out in an industrial size HTC-1000/4 ABS system (Hauzer Techno Coating, The Netherlands) shown schematically in Fig. 1. The chamber was equipped with four rectangular targets with an area of 1200 cm^2, which can be used in either CA or unbalanced magnetron (UBM) sputtering mode by adjustment of permanent magnets behind the targets.[13] A HIPIMS power supply HMP 2/4 [Advanced Converters (AC), Warsaw, Poland] with a peak power capability of 8 MW at 2 kV and arc suppression was additionally con-

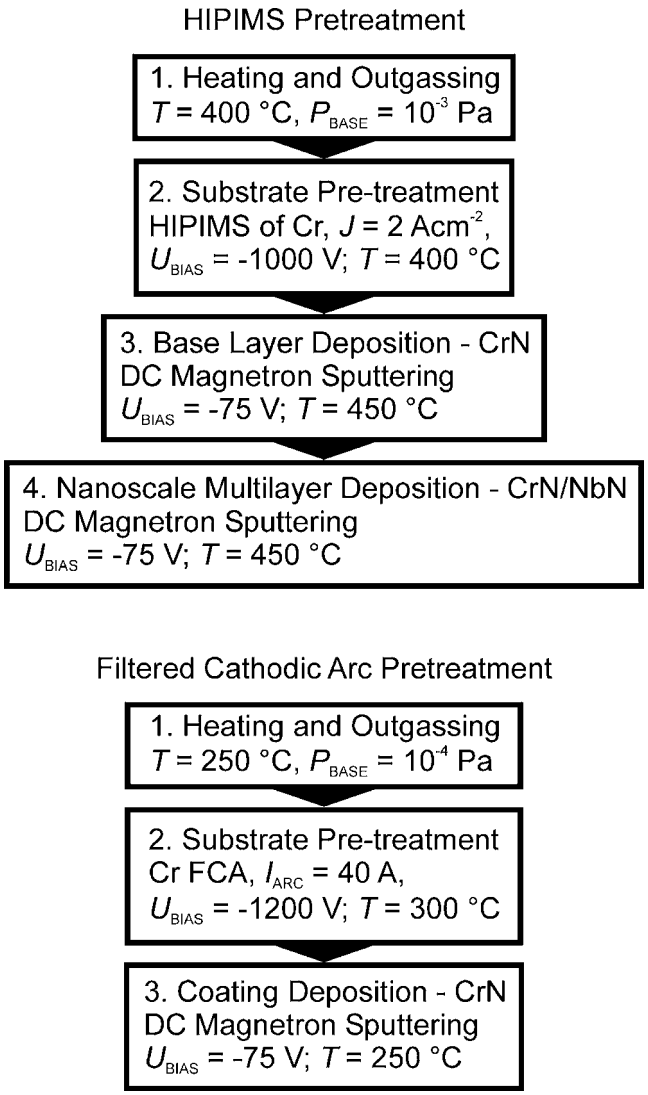

FIG. 2. Coating deposition sequence with pretreatment by HIPIMS (upper) and filtered cathodic arc (lower).

nected to one of the targets, allowing switching between CA/UBM and HIPIMS. The substrates were subject to threefold rotation.

The coating deposition sequence is shown in Fig. 2. The HIPIMS of Cr and Nb pretreatments utilized pulses with peak power densities of 1600 W cm^{-2} applied at the target at a duty cycle of 1%. The 304 stainless steel and M2 high speed steel substrates were biased to $U_{bias}=-600$ V and $U_{bias}=-1000$ V. The substrate temperature was maintained at 400 °C throughout the process by additional heaters and thermocouple monitoring.

The coating step was carried out by direct current (dc) sputtering in a reactive atmosphere of Ar and N_2 and comprised the deposition of a 0.3 μm thick CrN base layer followed by a 4 μm thick nanolayer structured CrN/NbN with a period of 3.4 nm. During deposition the total pressure was 0.4 Pa and the substrate bias was $U_{bias}=-75$ V. The substrates were heated to 400 °C. Further details are given by Hovsepian *et al.*[14]

Pretreatment in Ar glow discharge

The Ar pretreament was performed at a dc bias voltage of $U_{bias}=-1000$ V and an Ar pressure of 8×10^{-3} mbar. The four magnetrons were operated behind shutters at a low power of 0.5 kW to increase the plasma density near the substrates. The deposition of the CrN/NbN nanoscale multilayer coating was performed in the same equipment and at identical conditions as for HIPIMS pretreatment.

Pretreatment by unfiltered steered cathodic arc

The CA pretreatment was carried out at an arc current of 100 A dc. The substrates were biased to $U_{bias}=-1200$ V for substrate surface cleaning. The CA was operated in pure Ar atmosphere at a pressure of 0.12 Pa. The substrates were heated to a temperature of 400 °C, which increased to 500 °C during CA pretreatment. The deposition of the CrN/NbN nanoscale multilayer coating was performed in the same equipment and at identical conditions as for HIPIMS pretreatment.

Pretreatment by filtered cathodic arc

CrN coatings were prepared by a process comprising three steps—heating, pretreatment by Cr filtered cathodic arc (FCA), and coating deposition of CrN by reactive magnetron sputtering as outlined in the flow chart in Fig. 2. The coating deposition process was carried out in a laboratory vacuum chamber equipped with one dc FCA source and one dc magnetron sputtering source (3 in. diameter). The base pressure was 10^{-4} Pa (10^{-6} mbar). The arc filter was a 90° bend with an internal coil diameter of 80 mm. The substrate was stationary during pretreatment and deposition. The substrate was attached to a holder box and was heated from the back. The temperature was monitored *in situ* with a thermocouple attached to the side of the sample.

The samples were heated to 250 °C. The pretreatment was carried out for 4 min with an arc current of 40 A dc and a filter current of 350 A dc. The substrate bias was $U_{bias}=-1200$ V and the total substrate current density was 2 mA cm^{-2}. Argon was introduced at a low pressure of 0.1 Pa(1×10^{-3} mbar) to improve stability of the discharge. After the pretreatment step the substrate holder box was rotated such that the substrate faced the magnetron source and the deposition step was started. During deposition, the $Ar-N_2$ partial pressure ratio was $P_{Ar}:P_{N2}=1:1$. The flow of N_2 was adjusted to maintain a constant total pressure of 0.4 Pa(4×10^{-3} mbar). The substrate bias was −75 V.

Further details are given in Ref. 15.

Plasma and materials analyses

Diagnostics of the plasma composition at the substrate position at 200 mm from the cathode was carried out by energy-resolved mass spectroscopy utilizing a PSM003 instrument (Hiden Analytical Ltd.). The spectrometer was gated to collect data through the entire on time of the HIPIMS power pulse while off times were excluded.

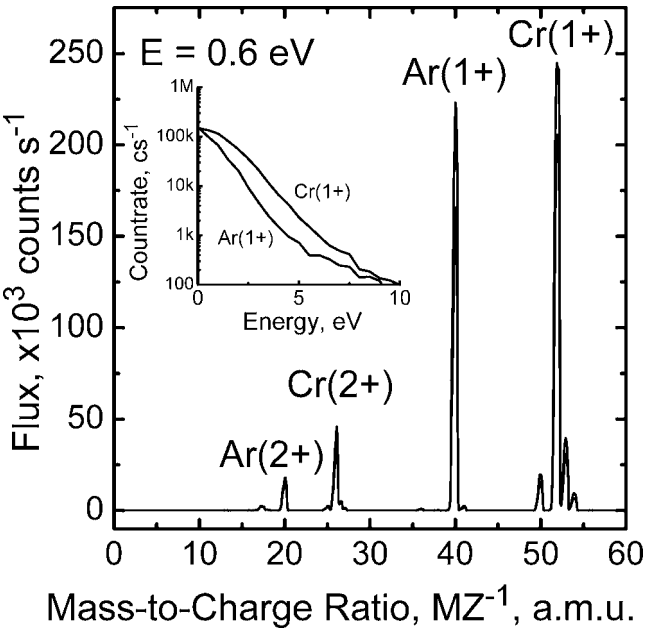

FIG. 3. Mass and energy spectra of the substrate ion flux generated by a HIPIMS of Cr discharge.

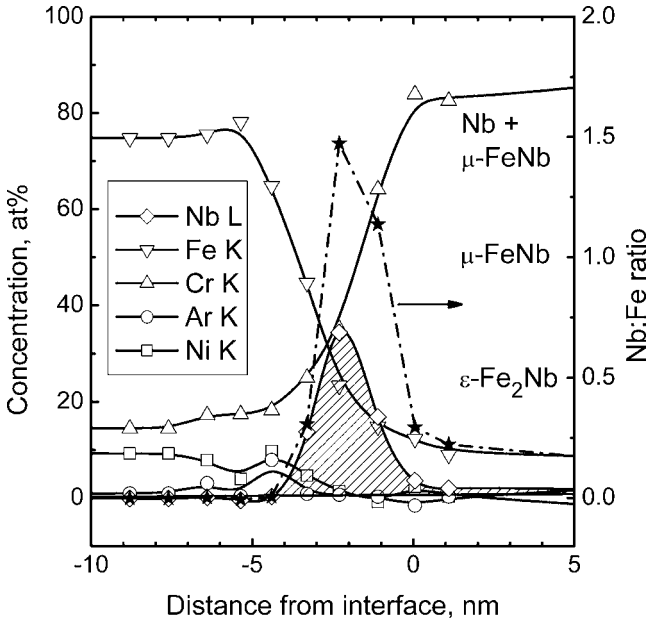

FIG. 4. Chemical composition of steel-CrN interface pretreated with HIPIMS of Nb at $U_{bias}=-1000$ V. Hollow symbols mark concentration in at. %. Stars represent the Nb:Fe ratio.

The ion flux to the substrates was measured with a flat electrostatic probe with a diameter of ø20 mm and was recorded with an oscilloscope to estimate the peak current during the pulse.

The chemistry of the coating-substrate interface was investigated with a scanning transmission electron microscopy energy dispersive x-ray (STEM-EDX) analysis technique. A dedicated STEM VG HB501 system with a field emission gun was used. The electron beam width was <0.3 nm, providing a spatial resolution for the analysis of 1 nm with provision for some spread within the sample.

The microstructure of the coating-substrate interface was observed by cross-sectional transmission electron microscopy (XTEM) (high-resolution TEM JEOL 2010F). The coating adhesion was determined in scratch testing (CSEM, Revetest) by optical observation of the scratch. The critical load L_C was defined as the first occurrence of the adhesive failure (spallation) of the film.

High speed steel (HSS) disks polished to $R_a=0.03$ μm were used to evaluate adhesion. TEM cross sections were carried out on polished 304 stainless steel squares.

RESULTS

Plasma properties

The magnitude of the ion flux was estimated with flat electrostatic probe measurements. During Ar pretreatment the current to the substrates was $j_S=0.2$ mA cm^{-2}. For the CA pretreatment $j_S=3$ mA cm^{-2}. During HIPIMS pretreatment, the peak pulse current to the substrates reached $j_S=300$ mA cm^{-2}. The average current was $j_S=3$ mA cm^{-2} (duty cycle of 1%). During coating the current was again $j_S=3$ mA cm^{-2}.

The chemistry of the ion flux during the HIPIMS pretreatment and UBM deposition process was estimated with energy-resolved mass spectroscopy. Figure 3 shows a mass spectrum collected at the substrate position during pretreatment by HIPIMS of Cr. The strongest peaks are from the singly ionized Cr^{1+} and Ar^{1+}. It is interesting to note that the metal ion to gas ion ratio is approximately 1. In contrast, for conventional UBM sputtering, the ratio was measured to be 0.1 for the same average power and gas pressure. Doubly charged species of Cr^{2+} and Ar^{2+} were also found in HIPIMS at levels of 10% and 5%, respectively. The metal-to-gas ion ratio observed for 2+ is higher than that for 1+ due to the lower ionization potential of Cr^{2+} compared to Ar^{2+}. The inset in Fig. 3 shows the energy distribution for singly charged ions; the doubly charged species had similar distributions (not shown). The average energy of all ions was ~ 2 eV with 95% of ions having energy less than 10 eV.

A similar high metal ion content was observed in HIPIMS of Nb targets at the power densities discussed in this paper. Optical emission spectroscopy (OES) observations[10] have demonstrated that the metal-to-neutral ion ratio was considerably higher for HIPIMS than for conventional UBM.

During coating deposition by conventional UBM, the ion flux was dominated by gas species with the following concentrations: N^+ (63%), N_2^+ (22%), and Ar^{1+} (1%). The Cr metal ion content at the substrate position was $<1\%$.

Interface: Chemical composition

The chemical composition of the coating-substrate interface was investigated for a system comprising three components: SS substrate, HIPIMS-Nb pretreatment, and CrN deposition. In this combination the incorporated element (Nb) is not present in the coating or substrate, which allows the spatial distribution to be well defined. The substrates were biased to $U_{bias}=-1000$ V in a HIPIMS of the Nb plasma environment.

Figure 4 shows the atomic concentration of elements as a function of distance from the interface. At the very inter-

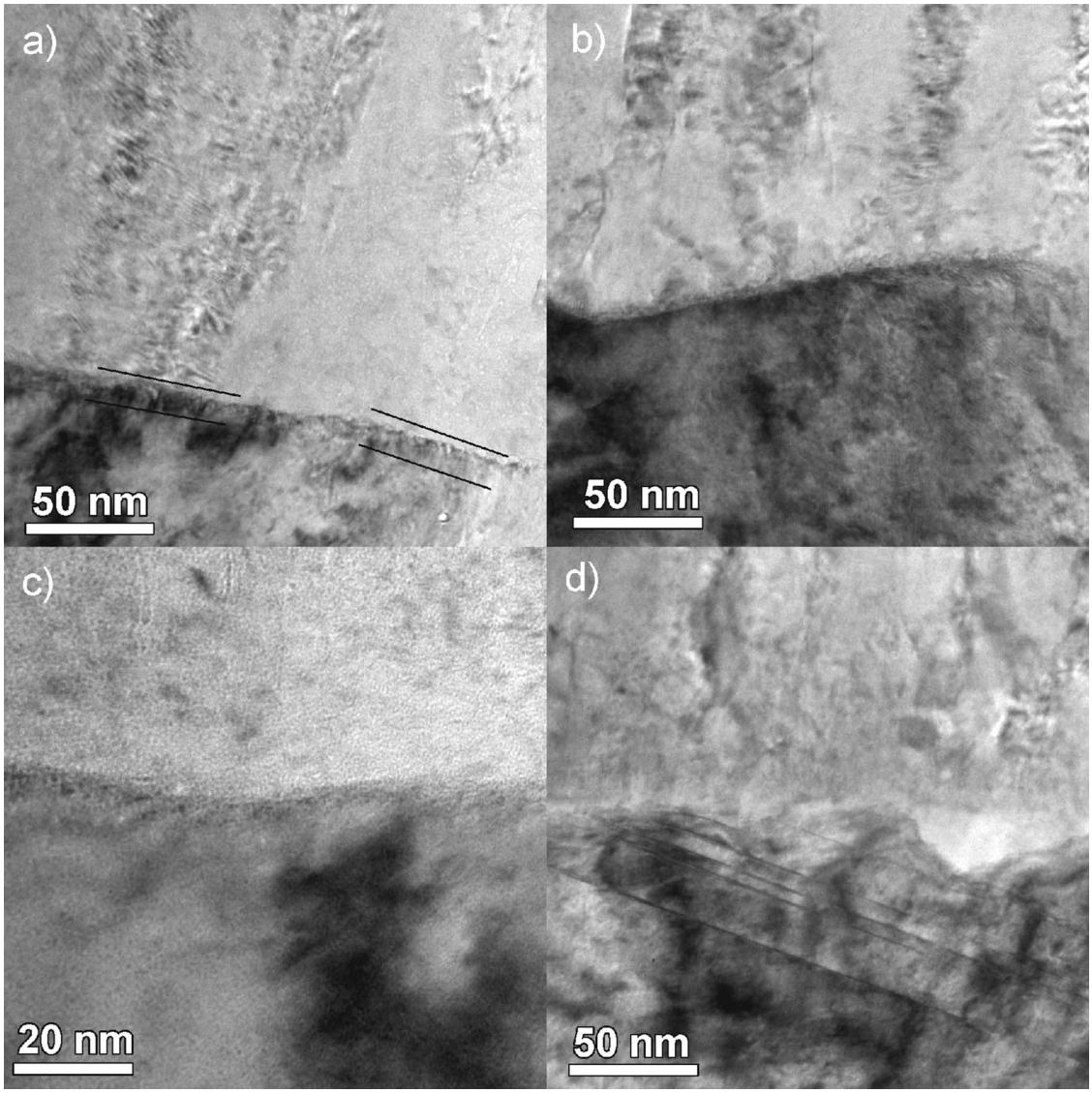

FIG. 5. Cross sectional views of interfaces prepared by (a) HIPIMS Cr pretreatment, $U_{bias}=-600$ V, (b) HIPIMS Cr pretreatment, $U_{bias}=-1000$ V, (c) HIPIMS Nb pretreatment, $U_{bias}=-1000$ V, and (d) Cr FCA pretreatment, $U_{bias}=-1200$ V.

face is a region with width of ~5 nm, where Nb is incorporated. The concentration of Ar is very low at <1 at. %.

The apparent ion range and content of Nb can be explained by the magnitude and chemistry of the ion flux. At a bombarding voltage of $U_{bias}=-1000$ V two phenomena occur—substrate resputtering and ion implantation. The substrate resputtering rate is significant because the sputter yield at 1000 eV is high, and at the same time the ion bombardment flux at the 300 mA cm^{-2} peak is substantial.

In conjunction, bombarding ions may be incorporated into the substrate to a significant depth of a few nanometers. Gas and metal ions have different behaviors when implanted. Implanted Ar gas atoms are inert and may be incorporated as interstitials in the substrate lattice or may interact with vacancies generated by the high energy bombardment and thus become substitutional. In either case the incorporation of Ar causes local increases in stress, which in turn embrittles the interface as it brings it closer to the yield stress.

In contrast, metal ions have a high bonding affinity and can be incorporated at lattice sites of the substrate as replacements. In the case of Nb implantation into Fe, the phases ε-Fe_2Nb and μ-FeNb are likely to form. In some systems such as Cr–Fe the solubility is full and there is no limit of the concentration that can be incorporated.

The ratio of Nb:Fe is plotted in Fig. 4. The maximum ratio found at the interface is 1.5, corresponding to a solid solution of the μ-FeNb phase and pure Nb. It should be noted that in this measurement Nb and Fe are always present at the same time, indicating that a pure Nb layer is not detected.

To elucidate the experimental observations of implanted Nb, dynamic transport of ions in matter (TRIM) simulations with the TRIDYN software[16] were performed. The results showed that for a metal-to-gas ion ratio $J(Ar^{1+}):J(Nb^{1+})=1:1$ and $U_{bias}=-1000$ V, no layer of Nb is formed. Both Nb and Ar are implanted in the steel substrate to a maximum ion range of approximately 4 nm. The simulation also shows that the probability of backscattering for Ar is a factor of 100 greater than for Nb. For Cr+Ar and V+Ar combinations the difference is a factor of 3. The number of reflected projectiles

depends on the atomic weight of the substrate material and the implanted layer with heavier substrate materials reflecting more. In addition to higher reflection, the inert nature of Ar and the presence of high energy metal ion bombardment favor radiation enhanced outdiffusion of the gas. Thus, experimentally, no detectable amounts of Ar are retained in the implanted layer. On the other hand, Nb—and also other metals in general—is highly reactive and is retained more readily. The simulation results on ion range and incorporation probability are consistent with the experimental measurement of interface chemistry presented in Fig. 4. The measured Nb concentration profile may thus be explained by the material implanted in the substrate. This implantation is a result of the high metal content in the ion flux and the high energy of bombardment given by the substrate voltage. The microstructure resulting from this incorporation is discussed in the following sections.

Interface: Microstructure

The microstructure of interfaces pretreated by HIPIMS of Cr and Nb was compared to the pretreatment by FCA of Cr.

Figure 5(a) shows the interface between the CrN base layer and the stainless steel substrate pretreated with $U_{bias}=-600$ V, which appears abrupt with a well defined boundary. At higher magnifications a band of a speckled contrast with a thickness of ~5–10 nm can be discerned within the substrate immediately below the interface, which is outlined in the figure. This band is produced during the pretreatment step and is a result of the high energy ion bombardment. The speckled contrast arises from lattice strain due to radiation damage induced by the metal ion implantation. The interface is generally clean and contains no foreign or amorphous phases due to contamination.

A similar structure is also observed for the substrates pretreated at $U_{bias}=-1000$ V in HIPIMS of the Cr environment. Figure 5(b) shows the interface region and a band with speckled contrast. The band here is larger (10–15 nm) than for the pretreatment at $U_{bias}=-600$ V, which is due to the higher energy and an associated longer range of implantation of bombarding ions.

Figure 5(c) is a cross section of the interface prepared by pretreatment in HIPIMS of the Nb environment at $U_{bias}=-1000$ V. The interface is clean and dense. A band of speckled contrast similar in width as HIPIMS Cr pretreatment at $U_{bias}=-1000$ V is visible.

The pretreatment by FCA resulted again in a clean interface with a 10 nm thick band with speckled contrast, as shown in Fig. 5(d). The thickness of the modified area is consistent with the high energy of bombardment and indicates a zone of high defect density.

The four interfaces presented in Figs. 5(a)–5(d) and discussed above are clean and dense as a result of the highly intensive bombardment flux containing high fractions of metal ions. It can be expected that these interfaces provide a direct contact between the coating and the substrate and thus promote the formation of the metallic, covalent, or ionic bonds as opposed to the significantly weaker van der Waals bonds.

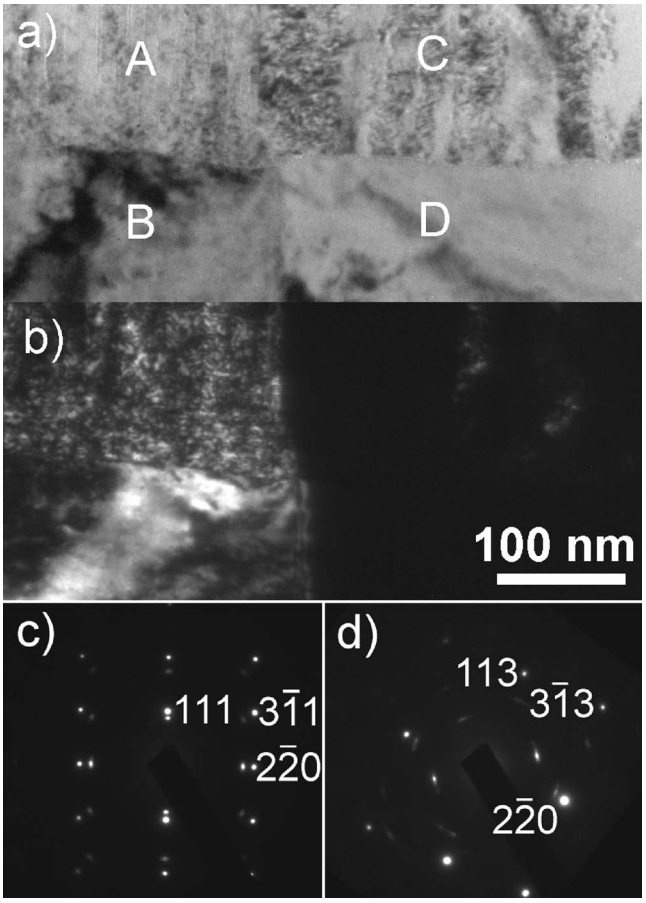

FIG. 6. TEM cross section of a CrN base layer grown on 304 stainless steel after HIPIMS Nb pretreatment at $U_{bias}=-1000$ V. (a) Bright- and (b) dark field images at the interface show the influence growth from the substrate. (c) The left and right selected-area diffraction patterns are from A+B region and C+D regions, respectively.

Local epitaxy on large areas: HIPIMS pretreatment

Larger lengths of the substrate-coating interface were examined. The interfaces considered were HIPIMS of Nb pretreated at $U_{bias}=-1000$ V. Figure 6(a) shows a sample region containing a grain boundary in the substrate. The sample is tilted such that a zone axis of the left grain is aligned with the beam, thus exciting that grain. At the same time the right grain remains away from its zone axis and is therefore not excited. The dark field image of this area [Fig. 6(b)] shows clearly a bright contrast from the left substrate grain, while the one on the right is completely dark. The white contrast of the excited left substrate grain is transferred across the interface to the coating grains, indicating that the coating has a similar orientation as the substrate. The right hand side substrate grain is fully dark (no excitation), and so is the coating structure above. From the dark field image it is evident that the switch in coating orientation is localized exactly at the substrate grain boundary where the switch in substrate orientation also occurs.

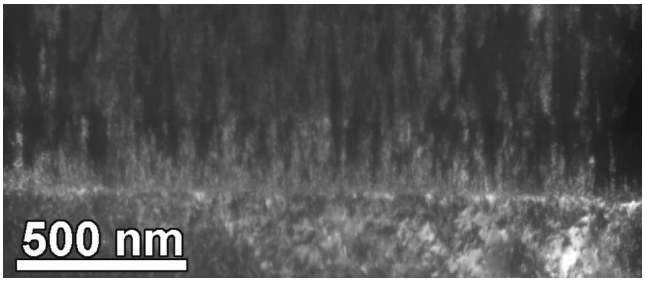

FIG. 7. Low magnification cross sectional dark field image of the interface.

The particular orientation of the substrate and coating grains was evaluated with selected-area diffraction patterns (SADPs). Figure 6(c) is SADP taken from the interface between grains A and B marked in Fig. 6(a), i.e., to the left of the substrate grain boundary. The diffraction pattern shows double reflections indexed as $[1\bar{1}2]$ zone axis of both film and substrate grains. The sharp reflections at the larger distance from the transmitted beam (smaller lattice size a_{SS} =0.359 nm) belong to the fcc stainless steel substrate. The set of reflections at a smaller distance (larger lattice size a_{CrN}=0.415 nm) belongs to the CrN base layer. In contrast to the substrate reflections, the coating ones are more arclike with a relatively small full width at half maximum (FWHM) intensity of 2.5° due to mosaicity in the in the film grain. The diffraction pattern shows unambiguously the cube-on-cube epitaxial orientation between the substrate and coating with good alignment between substrate and film, which is particularly interesting given the large lattice mismatch of 15%. The substrate grain B is oriented with a low index direction of [111] parallel to the substrate normal which may facilitate the good local epitaxy. Figure 6(d) is a SADP taken from grains C and D in Fig. 6(a), i.e., to the right of the substrate grain boundary. Here, the substrate grain is oriented with a $[33\bar{2}]$ zone axis parallel to the beam direction, while the low index 113 direction is at 21° with respect to the surface normal. The film zone axis is 001, with a parallel beam direction of $[33\bar{2}]$. The 220 reflections of the coating and the substrate

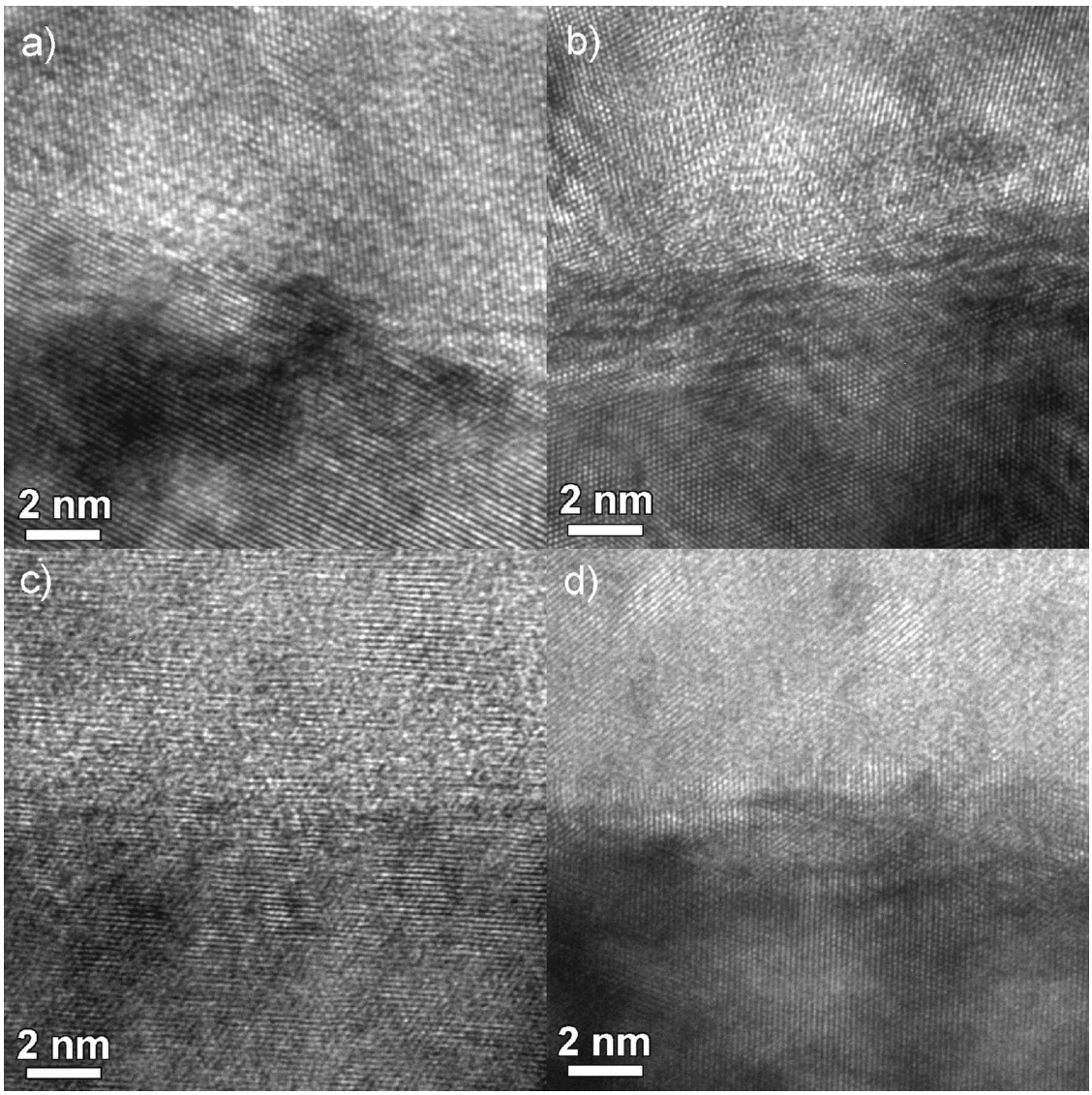

FIG. 8. Cross sectional lattice imaging of interfaces prepared by (a) HIPIMS of Cr pretreatment, U_{bias}=−600 V, (b) HIPIMS of Cr pretreatment, U_{bias} =−1000 V, (c) HIPIMS of Nb pretreatment, U_{bias}=−1000 V, and (d) Cr FCA pretreatment, U_{bias}=−1200 V.

are mutually aligned. The film reflection in this case are pronounced arcs with a disorientation of $>5°$. We find that the situation presented in Fig. 6 is typical, where substrate grains exposing low index planes promote cube-on-cube epitaxy while high index planes promote epitaxy on one coincident set of planes. The latter case is known as axiotaxy.[19] It has been shown that in cases when the substrate and coating planes have a high lattice mismatch, a clean interface with intimate bonding can still force the first monolayers to crystallize in a structure similar to the substrate. The growth proceeds in a tilted direction at an angle θ to the normal such that the atomic distance in the coating will match that of the substrate. The angle is given by $\cos(\theta)=b/a$, where a is the lattice spacing of the substrate and b is the lattice spacing of the coating.

Figure 7 shows a larger area of the interface region in a dark field imaging mode taken with an aligned substrate-film pair of reflections, similar to the one presented in Fig. 6(d). The interface region is highly excited and shows a white contrast that encompasses the coating and substrate. Significantly, the contrast is distributed over the whole length of observation of 3 μm, indicating a good alignment between coating and substrate along the full length of the observed area. Above several hundred nanometers into the coating the varied contrast indicates that the defective epitaxial grain has broken into polycrystalline columnar grains.

Lattice imaging of the interface region reveals further details of bonding.

Lattice imaging of the interface and local epitaxy

Figure 8(a) shows a lattice image of an interface prepared by HIPIMS of Cr with $U_{\text{bias}}=-600$ V. Atomic columns are resolved in both the coating and the substrate, indicating atomic registry between the two lattices. The interface can be distinguished by the apparent difference in angle of orientation between the lattice fringes of the substrate and the coating. The crystalline structure is preserved throughout the interface region. The atomic planes of the coating are seen to be in direct contact with the atomic planes of the SS substrates throughout the imaged area, thus signifying a fully dense interface. This level of contact can be compared to a grain boundary in bulk materials. No apparent gas accumulation and bubble formation were present.

Figure 8(b) shows a lattice image of the interface prepared at $U_{\text{bias}}=-1000$ V in HIPIMS of the Cr environment. The interface microstructure is modified compared to the $U_{\text{bias}}=-600$ V case. In the substrate a damage zone of 5–10 nm is visible by a slightly disturbed order in the lattice structure near the interface. Still, looking at the coating, the atomic columns are clearly resolved along both lattice vectors, thus indicating crystallographic registry to the substrate. Such a close match can rarely be obtained by chance especially in randomly oriented substrates and when, for example, an amorphous (or amorphized) layer prevents the influence of substrate on the coating.

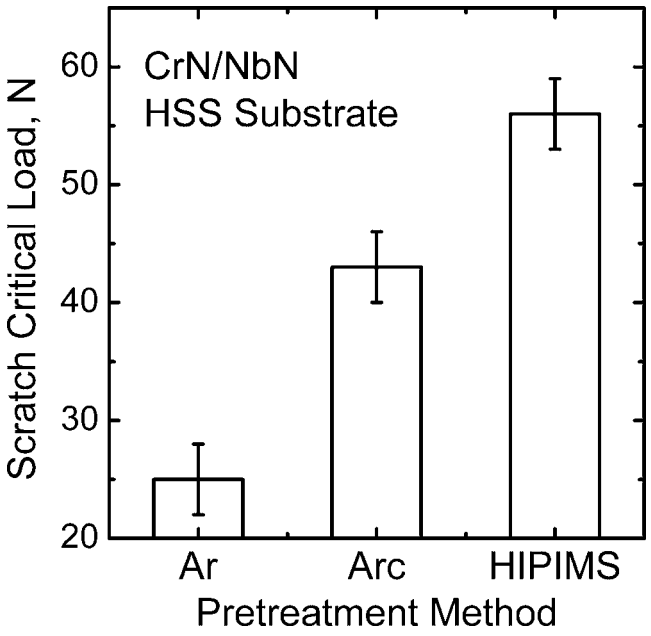

FIG. 9. Adhesion of CrN/NbN coatings on HSS substrate pretreated by Ar glow discharge, cathodic arc, and HIPIMS discharges.

The orientation alignment shown above was also observed for HIPIMS Nb pretreatment. As shown in Fig. 8(c), the lattice fringes of the SS substrate are transferred through the HIPIMS interface to the CrN coating.

The registry in crystal orientation between the substrate and coating was visible over large areas of micrometer size of the sample, and the images are representative of the long range structure despite showing an area of some tens of nanometers only. This is strong evidence pointing towards local epitaxy.

Clean interfaces were also generated by pretreatment by FCA. Figure 8(d) presents a lattice image of the substrate-coating interface. The interface is clean and no amorphous layer is observed. The substrate lattice planes are disturbed and bent in the first 6 nm adjacent to the interface. A number of misfit dislocations are observed at the very interface. In general, however, the interface is fully dense and is expected to have a high bonding strength.

In all cases the substrate grain lattice is more ordered, while the film lattice fringes are somewhat disordered, indicating defective epitaxy. While Fig. 8(c) is from a region with a cube-on-cube epitaxy, the rest of the lattice-resolution images indicate a rotation of the coating planes to match the planes of the substrate grains exposed to the surface in an axiotaxial fashion.

Adhesion

The large-scale epitaxy discussed in the previous section is expected to translate into strong adhesion of the overall coating as measured with scratch testing. Figure 9 presents a comparison between scratch test critical loads L_C for identical CrN/NbN nanolayered coatings where the interface was prepared by three methods of pretreatment: Ar glow discharge, Cr CA, and HIPIMS of Cr. The L_C values for HIPIMS pretreatment are higher than those for arc pretreatment.

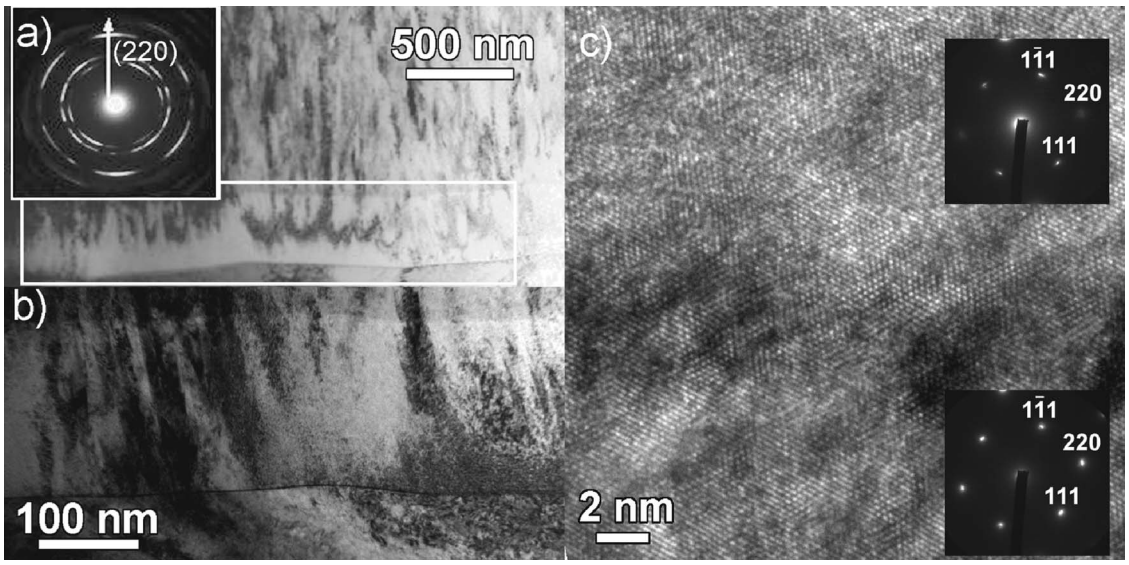

FIG. 10. Cross sectional views of the interface region of (a) TiAlN grown on SS304 after HIPMS of V pretreatment $U_{bias}=-1000$ V and (b) CrAlN coating on γ-TiAl with pretreatment of HIPIMS of Cr at $U_{bias}=-600$ V.

The difference may be attributed in part to the more disturbed nature of the arc interface as described in the previous section [Fig. 6(d)]. The Ar pretreatment resulted in a low adhesion due to the insufficient cleanliness of the interface and the embrittlement caused by the incorporation of Ar.

DISCUSSION

The structure and microchemistry of the pretreated surface are determined in part by the balance of metal ion implantation and resputtering. Diffusion plays a significant role. However, it is mainly affected by the temperature of the substrate[20] and thus can be considered constant when the energy and flux of ions change. The implantation depths of singly charged ions at the 600–1000 eV energies discussed are in the range of 5–8 nm. An analytical model by Carr *et al.*[20] predicts that the in-depth distribution of implanted ion concentration can be described with the logarithm of an error function. The authors show that the surface and maximum concentration is a function of resputtering efficiency and retention probability. The depth is controlled by the energy of the implanted species. In real processes, the rate of resputtering is governed by the magnitude of the ion flux. The energy of ions is given by the product of the bias voltage and the charge state. Thus, treatments that are carried out in the presence of highly charged metal ions can produce deeper implantation profiles. A typical example for discharges containing highly charged metal ions are CAs, where the average charge state is 2.05 for Cr and 2.5 for Nb with the maximum charge states for Nb of 5+. When electromagnetic macroparticle filters are used, higher ionization states are favored due to the limited expansion of the cathode spot plasma by the magnetic field, leading to an extended time of ionization before equilibrium described as freezing of the charge state distribution is reached.[17] The average charge state in the presence of magnetic field with shape similar to that in a filter can increase to 3.5 and 4 for Cr and Nb, respectively.[17] These highly charged metal ions gain significant energy in the biased substrate sheath and can have a very high range. This is illustrated by the large implanted zone shown in Fig. 6(d). Dynamic TRIM simulations[16] predict a penetration depth of 8 nm for Cr^{2+} in steel, which proportionally increases with charge state, and for Cr^{4+} the ion range is 15 nm. In this case the implanted species may cause irradiation damage relatively deep into the substrate. In some cases a nanocrystalline/amorphous layer can be formed.[18] Such layers act as a crystallographically neutral substrate and thus inhibits epitaxy.

The apparent coherency of the coating lattice to that of the substrate presented in Figs. 6–8 may be explained by the intimate bonding between the nitride coating and the substrate. As the nitride layer nucleates, the clean surface promotes direct bonding of the adatoms to the substrate with individual nuclei highly aligned over individual substrate grains due to crystallographic templating. During coalescence the film nuclei merge without forming grain boundaries. Thus, the grain size of the coating closely duplicates the structure of the substrate which typically is on the order of micrometers. This mode of interface formation is markedly different from cases when the coating nucleates on substrate grains covered with a layer that is amorphized or fine grained because of contamination or excessive ion damage. In addition to forming weaker bonding across the interface, the coating nuclei are randomly oriented in the plane of the film and form high-angle grain boundaries during coalescence, thus defining a column size in the nanometer or tens of nanometer range, as shown in Refs. 5 and 2.

Crystallographic templating by cube-on-cube epitaxy or axiotaxy can be observed for a wide range of crystalline substrate-coating pairs as long as the interface is free of impurities and amorphous contamination. For example, templating was observed for several coating-substrate combinations, e.g., $Ti_{0.5}Al_{0.5}N$ base layer on stainless steel with pretreatment by HIPIMS of V shown in Fig. 10(a) as well as for a CrAlN layer grown on the γ-TiAl substrate after HIPIMS Cr pretreatment shown in Figs. 10(b) and 10(c). The

$Ti_{0.5}Al_{0.5}N$ appears with uniform diffraction contrast in the bright-field TEM image [Fig. 10(a)] indicative of a large crystal grain growth as an extension to the substrate grain which is analogous to the interface structure shown in Fig. 7. The dark bands within the film are bend contours within the single crystal. The STEM image in Fig. 10(b) shows that the coating adjacent to the interface appears as a mirror image of the substrate. Figure 10(c) shows the crystalline epitaxial microstructure at the interface with cube-on-cube epitaxial relationship. The γ-TiAl substrate has a tetragonal structure with parameters $a=0.398$ nm and $c=0.407$ nm, which are close to the lattice parameters of CrN of $a_{CrN}=0.415$ nm. Although no crystallographic data were found for the CrAlN phase, thin film growth studies using cathodic arc evaporation have shown that the structure is similar to CrN up to a Cr:Al ratio of 2:3 and the lattice parameter is decreased to 0.413 nm for arc deposited coatings.[21] The small mismatch of 4% and 2% for a and c, respectively, is a strong condition promoting epitaxial growth.

In practice, substrate surfaces are contaminated and plasma pretreatment is a necessary step to achieve a high level of cleanness. It is beneficial to avoid inert gas ion etching due to incorporation in the substrate and the associated embrittlement due to high strains and coalescence into gas bubbles. When metal ions are used during pretreatment, they can be implanted and incorporated in the substrate as replacements, sometimes forming phases. Metal ion irradiation provides intense mixing in the near surface region which promotes radiation enhanced diffusion which provides an escape path for the implanted inert ion which in the case of HIPIMS are with a ratio of 1:1 with the metal gas ions. Metal ion incorporation in a HIPIMS plasma environment preserves the crystallinity and provides a high density interface with a good adhesion strength.

CONCLUSIONS

The paper illustrates the utilization of the high power impulse magnetron sputtering (HIPIMS) technology for the pretreatment of substrates prior to nitride coating deposition. Substrates were pretreated under high energy bombardment in a HIPIMS environment prior to coating deposition. The interface chemistry and microstructure were discussed in relation to the adhesion of the coatings.

HIPIMS was found to produce a highly ionized plasma containing equal amounts of metal and gas ions. The interface was free of contamination and amorphous phases such as native oxides. This provided a fully crystalline microstructure at the coating-substrate interface. The high content of metal ions in the bombarding flux modified the interface to include a metal implantation zone that promoted a strong bond between the substrate and the subsequently deposited coating. The clean interface and metal implantation zone promoted the alignment of the coating growth orientation to the crystal orientation of the substrate in at least one direction (axiotaxial growth). The coating orientation was observed to follow that of the substrate over large areas of several micrometers. It was also shown that the coating orientation mirrored changes in orientation at substrate grain boundaries.

Overall coatings deposited after HIPIMS pretreatment exhibited superior adhesion in comparison to pretreatments in Ar glow discharge and cathodic vacuum arc environments.

ACKNOWLEDGMENTS

The authors gratefully acknowledge Professor Papken Hovsepian from Sheffield Hallam University, UK and Professor Peter Barna, MFA, Hungary for stimulating discussions. Dr. Andre Anders of Lawrence Berkeley National Laboratory is acknowledged for the pretreatment by filtered cathodic arc. The financial support of the EU project INNOVATIAL is acknowledged. Two of the authors (J.G.W. and I.P.) are supported by U.S. Department of Energy under Grant No. DEFG02-91-ER45439.

[1] P. Hovsepian, Arch. Metall. **33**, 4 (1988).
[2] C. Schonjahn, A. P. Ehiasarian, D. B. Lewis, R. New, W. D. Munz, R. D. Twesten, and I. Petrov, J. Vac. Sci. Technol. A **19**, 4 (2001).
[3] G. Hakansson, L. Hultman, J.-E. Sundgren, J. E. Greene, and W.-D. Muenz, Surf. Coat. Technol. **48**, 1 (1991).
[4] C. Schonjahn, L. A. Donohue, D. B. Lewis, W.-D. Munz, R. D. Twesten, and I. Petrov, J. Vac. Sci. Technol. A **18**, 4 (2000).
[5] I. Petrov, P. Losbichler, D. Bergstrom, J. E. Greene, W.-D. Munz, T. Hurkmans, and T. Trinh, Thin Solid Films **302**, 1 (1997).
[6] V. Kouznetsov, K. Macak, M. Schneider, J. U. Helmersson, and I. Petrov, Surf. Coat. Technol. **122**, 2 (1999).
[7] A. P. Ehiasarian, R. New, W.-D. Munz, L. Hultman, U. Helmersson, and V. Kouznetsov, Vacuum **65**, 2 (2002).
[8] A. P. Ehiasarian, Y. A. Gonzalvo, and T. Whitmore, Plasma Processes Polym. (to be published).
[9] A. P. Ehiasarian, W.-D. Munz, L. Hultman, U. Helmersson, and I. Petrov, Surf. Coat. Technol. **163–164**, 267 (2003).
[10] A. P. Ehiasarian, P. E. Hovsepian, L. Hultman, and U. Helmersson, Thin Solid Films **457**, 2 (2004).
[11] C. Reinhard, A. P. Ehiasarian, and P. Eh. Hovsepian, Thin Solid Films **515**, 3685 (2007).
[12] W.-D. Munz, A. P. Ehiasarian, and P. E. Hovsepian, European Patent No. EP1260603B1 (2006).
[13] W.-D. Munz, D. Schulze, and F. J. M. Hauzer, Surf. Coat. Technol. **50**, 2 (1992).
[14] P. E. Hovsepian, D. B. Lewis, and W. D. Munz, Surf. Coat. Technol. **133–134**, 166 (2000).
[15] A. P. Ehiasarian, A. Anders, and I. Petrov, J. Vac. Sci. Technol. A (submitted).
[16] W. Moller, W. Eckstein, and J. P. Biersack, Comput. Phys. Commun. **51**, 3 (1988).
[17] E. M. Oks, A. Anders, M. R. Dickinson, and R. A. MacGill, IEEE Trans. Plasma Sci. **24**, 1174 (1996).
[18] C. Schonjahn, H. Paritong, W.-D. Munz, R. D. Twesten, and I. Petrov, J. Vac. Sci. Technol. A **19**, 4 (2001).
[19] C. Detavernier, A. S. Ozcan, J. Jordan-Sweet, E. A. Stach, J. Tersoff, F. M. Ross, and C. Lavoie, Nature (London) **426**, 6967 (2003).
[20] W. Carr, M. Seidl, G. S. Tompa, and A. Souzis, J. Vac. Sci. Technol. A **5**, 1250 (1987).
[21] H. Hasegawa, M. Kawate, and T. Suzuki, Surf. Coat. Technol. **200**, 2409 (2005).